Acta Astronautica 236 (2025) 514–521

Contents lists available at ScienceDirect

Acta Astronautica

journal homepage: www.elsevier.com/locate/actaastro

# EclipseNETs: Learning irregular small celestial body silhouettes

Giacomo Acciarini [a,b,*], Dario Izzo [a], Francesco Biscani [c]

[a] *European Space Agency, Advanced Concepts Team, Keplerlaan 1, 2201 AZ, Noordwijk, Netherlands*
[b] *Surrey Space Centre, University of Surrey, Stag Hill, University Campus, GU2 7XH, Guildford, United Kingdom*
[c] *Skylon Dynamics, Kurpfalzstrasse 4a, 75053 Gondelsheim, Germany*

## ARTICLE INFO

*Keywords:*
Small bodies
Silhouette reconstruction
Asteroids
Comets
NeuralODE
Neural events
Machine learning
Artificial intelligence
AI for space
Spaceflight mechanics
Orbital dynamics

## ABSTRACT

Accurately predicting eclipse events around irregular small bodies is crucial for spacecraft navigation, orbit determination, and spacecraft systems management. This paper introduces a novel approach leveraging neural implicit representations to model eclipse conditions efficiently and reliably. We propose neural network architectures that capture the complex silhouettes of asteroids and comets with high precision. Tested on four well-characterized bodies - Bennu, Itokawa, 67P/Churyumov-Gerasimenko, and Eros - our method achieves accuracy comparable to traditional ray-tracing techniques while offering orders of magnitude faster performance. Additionally, we develop an indirect learning framework that trains these models directly from sparse trajectory data using Neural Ordinary Differential Equations, removing the requirement to have prior knowledge of an accurate shape model. This approach allows for the continuous refinement of eclipse predictions, progressively reducing errors and improving accuracy as new trajectory data is incorporated.

## 1. Introduction

Small celestial bodies, including asteroids and comets, play a critical role in space exploration. They provide insights into the early Solar System, offer potential resources for future missions, and pose impact threats to Earth [1,2]. As remnants of Solar System formation, they preserve primordial materials that inform our understanding of early chemical and physical conditions. Additionally, they present unique opportunities for scientific exploration, such as sample-return missions and spacecraft technology testing [3–6]. As their exploration becomes more advanced, understanding the dynamics of spacecraft as they orbit or interact with these bodies is critical, particularly given their irregular shapes, weak gravity, and complex physical properties [7].

Precise eclipse condition estimation is vital in small-body exploration, impacting solar radiation pressure calculations, communication, and spacecraft thermal and power management [8–10]. For objects with high area-to-mass ratios orbiting weak-gravity bodies, solar radiation pressure is a dominant perturbation, making accurate eclipse computation essential for predicting spacecraft motion [11–13].

Eclipse computation involves determining whether an orbiting object's position lies within a celestial body's shadow [14]. Shadow modeling depends on the body's shape and size; simple bodies allow for approximations using cylindrical cones, while irregular bodies require high-fidelity 3D models [15]. For example, the NASA OSIRIS-REx mission employed a detailed 3D model of asteroid 101955 Bennu to simulate the precise shadow region and the motion of ejected particles [13,16].

Traditional eclipse modeling methods, such as the Möller–Trumbore intersection algorithm [17], use ray-tracing techniques to determine shadow regions. While highly accurate, these methods are computationally expensive and non-differentiable, limiting their utility in reliably estimating eclipse entrance and exit conditions [18]. Recent advances in neural image processing introduce differentiable and computationally efficient alternatives using implicit neural representations, particularly Neural Radiance Fields (NeRFs). These models capture complex 3D scenes with photometric consistency [19]. Periodic activation functions, as explored by Sitzmann et al. [20], enhance the ability to model high-frequency details, making them well-suited for accurately describing shadows cast by irregular celestial bodies [18,21].

In this paper, we construct a database of irregular silhouettes for four small celestial bodies using their shape models. The dataset is split into training and validation sets to train neural networks, termed EclipseNETs, for reconstructing small-body silhouettes from different

---

* Corresponding author at: Surrey Space Centre, University of Surrey, Stag Hill, University Campus, GU2 7XH, Guildford, United Kingdom.
*E-mail address:* giacomo.acciarini@gmail.com (G. Acciarini).

https://doi.org/10.1016/j.actaastro.2025.06.002
Received 31 March 2025; Received in revised form 23 May 2025; Accepted 2 June 2025

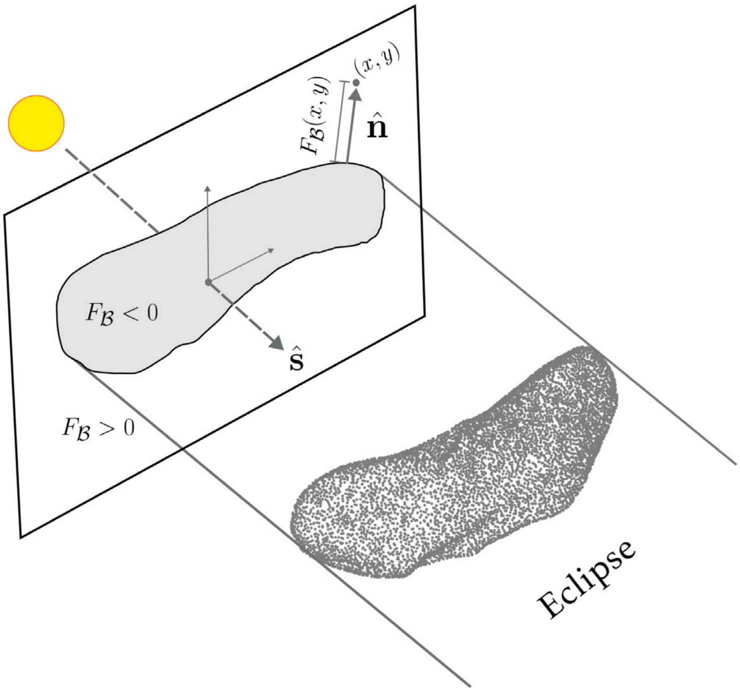

**Fig. 1.** Schematic illustration of the shadow cast by an irregular body, and its eclipse function $F_{\mathcal{B}}$.

directions. We first compare periodic activation functions with ReLU-based architectures confirming their superior ability in capturing complex shapes. Then, we integrate these models into orbital propagators to assess their accuracy and computational efficiency relative to traditional methods. The results demonstrate that EclipseNETs can efficiently and accurately perform eclipse condition computation. Due to the differentiable nature of EclipseNETs, this approach further facilitates the use of Taylor propagators [18], enhancing the reliability and accuracy of eclipse event detection during orbital propagation.

In the second part of the paper, we introduce a training technique based on Neural Ordinary Differential Equations (NeuralODEs) [22,23], which enables the direct learning of silhouettes from trajectory data. This approach eliminates the need for precise prior knowledge of the irregular shapes of small bodies, which are often not accurately known before in situ exploration. By incorporating EclipseNET, the resulting spacecraft dynamics can be formulated as a NeuralODE, allowing direct optimization of the network parameters from trajectory data. This enables learning and/or refinement of the eclipse model by minimizing trajectory prediction errors, presenting a novel strategy to improve irregular eclipse descriptions through NeuralODEs.

The paper is structured as follows: Section 2 discusses methods and related work, focusing on eclipse function definitions, the irregular bodies studied, and the spacecraft dynamics. Section 3 details the training process of EclipseNETs, comparing SIREN-based and ReLU-based architectures. We also discuss EclipseNET integration in a Taylor-based orbital propagator, benchmarking it against traditional ray-intersection methods. Section 4 introduces an algorithm for direct silhouette learning from trajectory data via NeuralODEs. Finally, Section 5 summarizes our findings.

## 2. Methods

### 2.1. Eclipse function

An eclipse function, $F_{\mathcal{B}}(x, y, \hat{\mathbf{s}})$, is introduced to implicitly represent the eclipsed region created by an irregular body $\mathcal{B}$ when illuminated by a point source at infinity in the direction $\hat{\mathbf{s}}$ (in the body frame). This function is defined in a reference frame lying in a plane orthogonal to $\hat{\mathbf{s}}$.

Mathematically, the eclipse function is given by:

$$F_{\mathcal{B}}(x, y, \hat{\mathbf{s}}) = \begin{cases} d(x, y, \partial\Omega_{\hat{\mathbf{s}}}) \text{ (outside the eclipse region)} \\ -d(x, y, \partial\Omega_{\hat{\mathbf{s}}}) \text{ (inside the eclipse region)} \end{cases}$$

where $d(x, y, \partial\Omega_{\hat{\mathbf{s}}})$ represents the signed distance function from the point $(x, y)$ to the boundary $\partial\Omega_{\hat{\mathbf{s}}}$ of the eclipse region. This function is closely related to the signed distance function, commonly used in computer graphics [24], but here it describes two-dimensional shapes parametrized by the projection direction $\hat{\mathbf{s}}$. The gradient of the eclipse function in the direction perpendicular to the eclipse boundary satisfies:

$$\nabla_{x,y} F_{\mathcal{B}} \cdot \hat{\mathbf{n}} = 1,$$

where $\hat{\mathbf{n}}$ is the unit normal (either outward or inward) to $\partial\Omega_{\hat{\mathbf{s}}}$. Fig. 1 provides a visual representation of the eclipse function and its relevant geometric properties. While Fig. 2 B) illustrates examples of the eclipse function for a specific direction across different bodies.

### 2.2. Irregular bodies

Our focus is on four different small bodies: 101955 Bennu, 67P/Churyumov - Gerasimenko, 433 Eros, and 25143 Itokawa. In all cases, high-fidelity polyhedral models reconstructed from various instruments on board spacecraft that visited these celestial bodies are utilized. For Eros and Itokawa, models produced by Robert Gaskell [25,26] are used; for Bennu, the model provided by the OSIRIS-REx team [27] is employed; and for Churyumov–Gerasimenko, the model available from the European Space Agency [28] is used.

To model the gravitational field of these bodies, the surface meshes are transformed into mascon models following the same procedure outlined in [29]. This is achieved by first generating a constrained Delaunay tetrahedralization [30] of the polyhedral mesh and then assigning a mass at the centroid of each resulting tetrahedron. Fig. 2 A) presents a 3D visualization of these models. The final representation of each asteroid consists of a triangular mesh that defines the surface geometry and a mascon model that describes the mass distribution, which is assumed to be uniform in all cases.

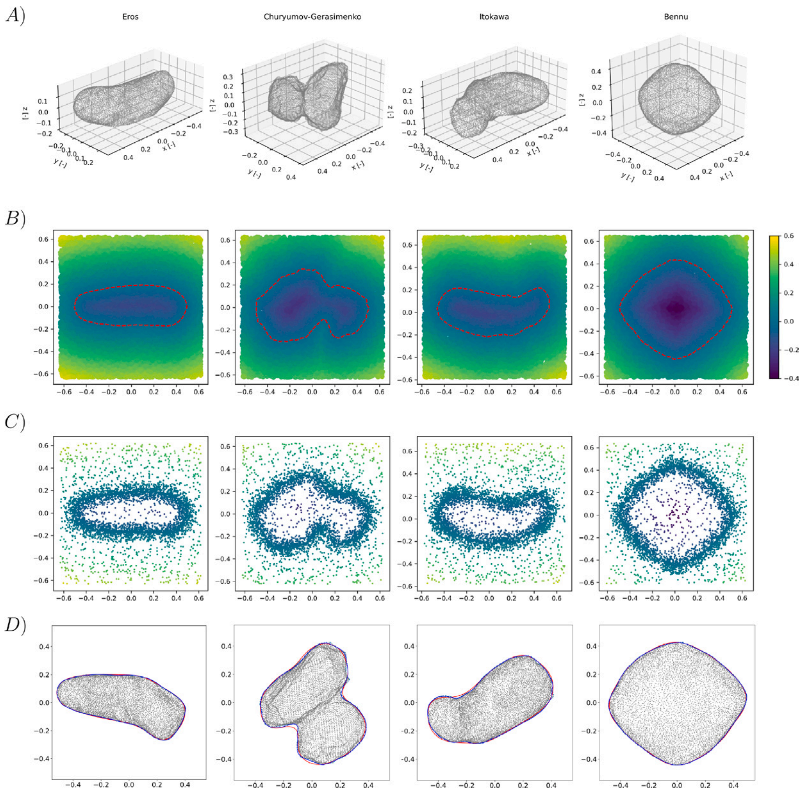

**Fig. 2.** (A) 3D models of Bennu, Churyumov-Gerasimenko, Eros, and Itokawa. (B) Contour plot of the eclipse function for a fixed viewpoint. (C) Sampled points of the eclipse function used to build the training set. (D) Eclipse predictions for a Sun direction not included in the training set. The red curve represents an EclipseNet with 2369 parameters, while the blue curve corresponds to 50,561 parameters. (For interpretation of the references to color in this figure legend, the reader is referred to the web version of this article.)

The resolution of these models, along with physical properties such as the rotation period and mass of each body, affects the dynamics of an orbiting spacecraft. The number of mesh points and mascons determines the fidelity of both the shape and gravitational field representation, while the rotation rate ($\omega$) influences orbital stability and eclipse conditions. A characteristic length scale ($L$) is used to normalize positional coordinates. Table 1 summarizes these key parameters for each of the four celestial bodies considered in this study.

**Table 1**
Key parameters of the 3D models used for small-body analysis.

| | N mesh | N mascons | $\omega$ [hr] | L [km] | mass [kg] |
|---|---|---|---|---|---|
| Bennu | 7,374 | 75,150 | 4.296 | 0.5634 | $7.329 \times 10^{10}$ |
| Itokawa | 3000 | 100,363 | 12.132 | 0.5607 | $3.51 \times 10^{10}$ |
| 67P | 9,149 | 57,259 | 12.4043 | 5.0025 | $9.982 \times 10^{12}$ |
| Eros | 7,374 | 97,824 | 5.270 | 32.6622 | $6.687 \times 10^{15}$ |

The 3D triangular mesh models are used to determine the ground truth eclipse conditions by applying the Möller–Trumbore intersection algorithm [17], which checks whether a ray from the light source intersects the body's surface, providing a ground truth for eclipse detection. Meanwhile, the mascon model is incorporated into trajectory simulations to account for the irregular gravitational field of each asteroid or comet. By combining these high-resolution shape models with a mascon distribution, we ensure an accurate and high-fidelity representation of the dynamical environment surrounding these small celestial bodies.

### *2.3. Spacecraft dynamics*

The spacecraft dynamics, taken from [18], is described in a body-centered reference frame by formulating the following set of differential equations:

$$\begin{cases} \dot{\boldsymbol{r}} &= \boldsymbol{v} \\ \dot{\boldsymbol{v}} &= -G \sum_{j=0}^{N} \frac{m_j}{|\boldsymbol{r} - \boldsymbol{r}_j|^3} (\boldsymbol{r} - \boldsymbol{r}_j) - 2\boldsymbol{\omega} \times \boldsymbol{v} - \boldsymbol{\omega} \times (\boldsymbol{\omega} \times \boldsymbol{r}) - \eta \nu(\boldsymbol{r}) \hat{\mathbf{s}}(t), \end{cases} \tag{1}$$

where $\boldsymbol{r}$, $\boldsymbol{v}$ denote the position and velocity vectors, respectively, of the spacecraft in the body-centered reference frame, $m_j$ and $\boldsymbol{r}_j$ represent the mass and position, respectively, of each mascon that characterizes the asteroid's irregular gravitational field, and $\boldsymbol{\omega}$ is the angular velocity of the asteroid's rotation. The term $\eta$ corresponds to the acceleration magnitude due to solar radiation pressure, which is modeled to be $10^{-3}$ m/s$^2$ for all simulations, while the term $\nu(\mathbf{r})$ represents the eclipse factor, which is considered as zero ($\nu = 0$) when the spacecraft is in eclipse and one ($\nu = 1$) otherwise. Traditional implementations use ray-tracing algorithms to determine the eclipse factor and to discontinuously change the dynamics. In this case, however, the aim is to substitute these algorithms with neural models. Hence, as detailed in Section 3, a small neural network, called EclipseNET, will be used to represent the eclipse factor. Then, $\boldsymbol{\omega} \times \mathbf{v}$, represents the Coriolis force, resulting from the rotational motion of the asteroid, and $\boldsymbol{\omega} \times (\boldsymbol{\omega} \times \mathbf{r})$ corresponds to the centrifugal force experienced due to the asteroid's rotation. Finally, the unit vector, $\hat{\mathbf{s}}(t)$, describes the direction of the Sun. The Sun direction is modeled as $\hat{\mathbf{s}}(t) = \mathbf{R}(t)\hat{\mathbf{s}}(0)$, where $\mathbf{R}(t)$ is the rotation matrix that evolves over time as the asteroid rotates at an angular velocity $\boldsymbol{\omega}$, causing a time-dependent change in the Sun's direction relative to the spacecraft. Using this model, we consider the Sun's direction as a simple rotation of the initial direction $\hat{\mathbf{s}}(0)$ by an angle $\omega t$. All these effects combine to determine the spacecraft's trajectory relative to the rotating asteroid reference frame.

## 3. Learning small body silhouettes with EclipseNET

To model the complex eclipse conditions caused by irregular small bodies, we introduce EclipseNET, a neural network architecture designed to implicitly represent the geometry of eclipses. Given the recent success of SIREN networks [20] in neural implicit representations of complex shapes, we compare EclipseNETs trained with ReLU and with periodic activation functions.

We write the EclipseNET as:

$$e_{\boldsymbol{\theta}} = \mathcal{N}_{\boldsymbol{\theta}}(\boldsymbol{r}, \hat{\mathbf{s}}) \tag{2}$$

where $\boldsymbol{r}$ is the positional vector of the spacecraft, and $\hat{\mathbf{s}}$ is the Sun direction. To facilitate the training, the state is projected onto the plane perpendicular to the Sun direction, and the two direction components of the projected spacecraft position are normalized and used as inputs, while the Sun direction is encoded using the sine and cosine of azimuth and elevation angles, making the total size of the network inputs six-dimensional. The output, $e_{\boldsymbol{\theta}}$, is a scalar value representing the eclipse function: negative when the spacecraft is in eclipse, positive when it is outside of eclipse, and zero at the asteroid silhouette.

To train EclipseNET, we create a dataset that contains ground truth values for the eclipse function found using the shape models of the small bodies. We consider an isotropic range of Sun directions, which is generated using the Fibonacci sphere. This results in 500 Sun directions for training and 200 for validation. For each direction, we uniformly sample 1000 points $(x, y)$ in the range $[-1, 1]$ and 3000 points around the eclipse boundary and an additional 3000 points concentrated around the eclipse boundary $\partial\Omega_{\hat{\mathbf{s}}}$. The latter are sampled uniformly within a circle of radius 0.01 (in non-dimensional units) centered on the boundary. An example of the result of this sampling procedure for the four small bodies in a random direction is shown in Fig. 2 C). This data yields a total of 22 million training points and 9 million validation points for each of the four small bodies studied.

We investigate the performance of two neural network architectures for training EclipseNETs: a sinusoidal representation network (SIREN) and a conventional ReLU-activated multilayer perceptron (MLP), each comprising 2369 trainable parameters. Rather than seeking an optimal network configuration for modeling the eclipse function, our objective is to assess whether highly compact neural architectures can leverage the expressive power of SIREN. The latter is a class of networks previously demonstrated to be effective for implicit neural representations in related tasks, such as encoding fine-grained geometric structures. As shown in Table 2, the SIREN-based architecture consistently outperforms its ReLU-based counterpart in both training and validation regimes at this parameter scale. Specifically, the SIREN model yields a lower mean squared error (MSE), indicating enhanced fidelity in capturing the intricate features of the eclipse silhouette boundary. To support this, Fig. 3 presents the MSE loss as a function of training epochs for both the SIREN and ReLU networks, for the 67P case. The figure includes two unseen views during training of the asteroid from the first and last epochs, along with their corresponding silhouette approximations, generated using the ReLU network (top, in orange) and the SIREN network (bottom, in blue). As observed, the SIREN network not only achieves lower loss levels than the ReLU network but also converges more quickly. This results in a more accurate silhouette reconstruction, particularly at the initial epoch, where the difference is noticeable. By the final epoch, the ReLU network reduces the gap to some extent but still struggles with sharp and irregular features in the shape.

While inspecting these losses and visually observing the accuracy of the silhouette reconstruction provides a good indication of the accuracy of the EclipseNET, it is however equally important to quantify what the resulting error in the state of a spacecraft orbiting these small bodies is, should the EclipseNET be used to identify eclipse regions. Formally, this means that when integrating Eq. (1), the eclipse factor is directly determined using the EclipseNET as an event function in the integrator. In this way, when the EclipseNET is zero, then the spacecraft is crossing the asteroid silhouette, which causes the eclipse factor to change value (from zero to one or vice-versa) if the spacecraft is behind the small body with respect to the Sun.

**Table 2**
Feed forward neural networks with ReLU activation function and SIREN network models mean squared error loss (MSE) on the training and validation datasets for all four small bodies.

| | $\mathcal{L}_{MSE}$ ReLU | $\mathcal{L}_{MSE}$ SIREN | Dataset |
|---|---|---|---|
| $\mathcal{N}_{Bennu}$ | $3.5295 \times 10^{-5}$ | $1.9906 \times 10^{-5}$ | $\mathcal{D}_{train,Bennu}$ |
| $\mathcal{N}_{Itokawa}$ | $8.0184 \times 10^{-5}$ | $4.7082 \times 10^{-5}$ | $\mathcal{D}_{train,Itokawa}$ |
| $\mathcal{N}_{67P}$ | $7.9564 \times 10^{-5}$ | $4.6469 \times 10^{-5}$ | $\mathcal{D}_{train,67P}$ |
| $\mathcal{N}_{Eros}$ | $9.3738 \times 10^{-5}$ | $4.2137 \times 10^{-5}$ | $\mathcal{D}_{train,Eros}$ |
| $\mathcal{N}_{Bennu}$ | $3.6508 \times 10^{-5}$ | $2.1773 \times 10^{-5}$ | $\mathcal{D}_{valid,Bennu}$ |
| $\mathcal{N}_{Itokawa}$ | $8.4136 \times 10^{-5}$ | $4.9863 \times 10^{-5}$ | $\mathcal{D}_{valid,Itokawa}$ |
| $\mathcal{N}_{67P}$ | $8.1466 \times 10^{-5}$ | $4.9408 \times 10^{-5}$ | $\mathcal{D}_{valid,67P}$ |
| $\mathcal{N}_{Eros}$ | $9.8826 \times 10^{-5}$ | $4.5850 \times 10^{-5}$ | $\mathcal{D}_{valid,Eros}$ |

In the first three columns of Fig. 4, we present three projections of three-dimensional orbits around the four tested small bodies, highlighting the entry and exit points of eclipses along the trajectory. For these experiments, the SIREN networks were used as EclipseNETs. As shown in the rightmost column, using these models to approximate the asteroid silhouette yields eclipse prediction errors within centimeters for all tested small bodies, even after multiple orbits. This accuracy is benchmarked against the eclipses computed using a ray-tracing method based on the Möller–Trumbore triangle intersection algorithm [17]. The computational efficiency of EclipseNET is remarkable, with inference speeds more than two orders of magnitude faster than the ray-tracing approach, demonstrating its potential to replace computationally expensive traditional algorithms in space-flight simulations.

While these results are promising, there will always be a slight discrepancy between the actual eclipse boundary and its representation by EclipseNET. This mismatch is expected to grow over time, particularly when the spacecraft traverses more complex eclipse regions or encounters irregular bodies with intricate geometries. Additionally, the irregular shape of small bodies is often not accurately known beforehand, and precise information about the body's shape may only become available as the spacecraft closely approaches the asteroid or comet.

Hence, there might be the need for continuous refinement and adaptability of the model's accuracy, as trajectory data become available. To address this, the next section introduces online training methods based on NeuralODEs [22]. These techniques allow the model to dynamically adjust in real-time, based on the evolving spacecraft trajectory, ensuring that the model becomes increasingly precise as it learns from positional data during the mission. Building upon this, the following section introduces how NeuralODEs can be employed to learn the silhouette of an irregular small body directly from trajectory data.

## 4. Learning the silhouette from trajectories via neuralodes

As discussed in the previous section, the shape of an irregular small body is often incompletely known or lacks sufficient resolution prior to a spacecraft visit. Even when a preliminary shape model is available, EclipseNET's implicit representation may contain inaccuracies that could lead to growing errors over time. Consequently, further model refinement is often necessary to ensure an acceptable error in predicting the satellite's position and velocity.

To address this challenge, we propose a method to dynamically learn and update the neural representation of the small body's silhouette directly from sparse trajectory data. This approach leverages NeuralODEs [22,31], specifically ODEs with neural event functions [23], to iteratively refine the eclipse function. This enables real-time and continuous adaptation of the model as new observational data becomes available.

As clarified in Section 2.3, the spacecraft dynamics changes according to a termination criterion triggered by an eclipse function, which in our case is modeled as a neural network (EclipseNET). Our objective is

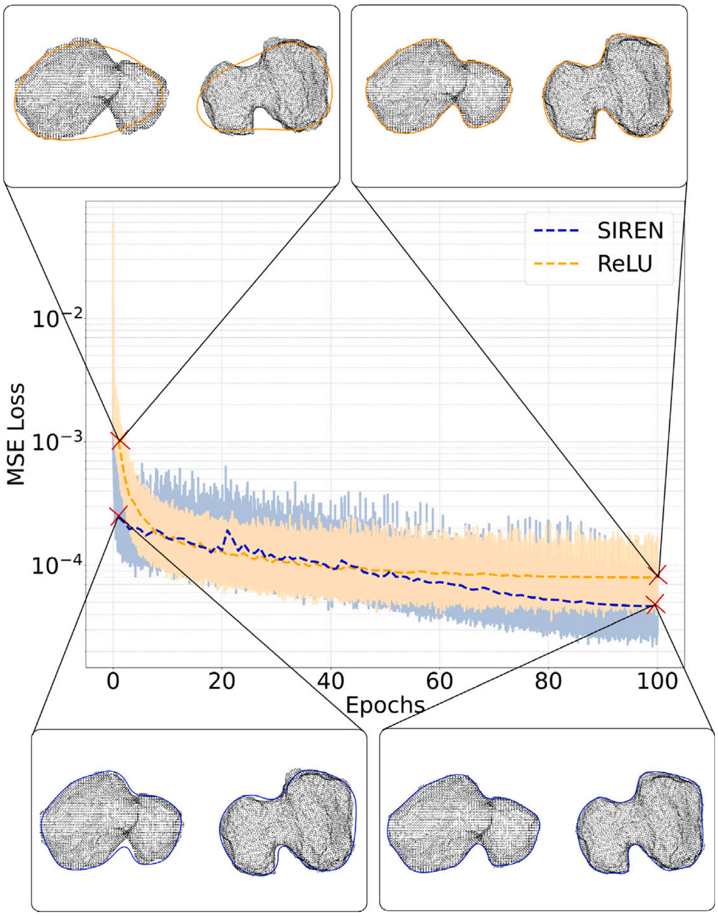

**Fig. 3.** Training loss vs the number of epochs, together with some views of the approximated silhouette for both networks at the first and last epochs, for both SIREN and ReLU networks, for the case of 67P/Churyumov–Gerasimenko.

to refine the EclipseNET used as a neural event function to reduce the observed errors in the spacecraft's states. To achieve this, we first define the augmented system dynamics, where the first-order ODE governing the satellite's motion in the small-body environment is extended with an equation for the event manifold time derivative:

$$\begin{cases} \dot{\boldsymbol{x}} &= \boldsymbol{f}_{\boldsymbol{\theta}}(t, \boldsymbol{x}) \\ \dot{\varepsilon}_{\boldsymbol{\theta}} &= g_{\boldsymbol{\theta}}(t, \boldsymbol{x}), \end{cases} \tag{3}$$

where the state is composed of the position and velocity of the spacecraft, $\boldsymbol{x} = [\boldsymbol{r}, \boldsymbol{v}]$ and the variable $\varepsilon_{\boldsymbol{\theta}}$ has been introduced to track the time derivative of the EclipseNET. The term $g_{\boldsymbol{\theta}}$ represents the total time derivative of the EclipseNET, which is a function of: $\boldsymbol{x}(t)$ and $\hat{\mathrm{s}}(t)$. Hence, using the chain rule, we can write:

$$g_{\boldsymbol{\theta}} = \nabla_{\hat{\mathrm{s}}} e_{\boldsymbol{\theta}} \cdot \dot{\hat{\mathrm{s}}}(t) + \nabla_{\boldsymbol{x}} e_{\boldsymbol{\theta}} \cdot \boldsymbol{f}_{\boldsymbol{\theta}}.$$

Under our assumptions, the derivative of the Sun direction can be found as: $\dot{\hat{\mathrm{s}}} = \dot{\mathbf{R}}(t)\hat{\mathrm{s}}(0)$. Hence, the first equation mirrors Eq. (1), while the EclipseNET, $e_{\boldsymbol{\theta}}$, acts as the event trigger function, to change the value of $\nu(\boldsymbol{r})$. The learnable parameters of the EclipseNET, $\boldsymbol{\theta} \in \mathbb{R}^m$, control the discontinuous transitions in the dynamics, with the subscript indicating this dependency. The outcome of this formulation is a NeuralODE wherein the neural network functions as a (differentiable) event manifold. It is important to emphasize that the event triggering in our framework is not influenced directly by the magnitude of the solar radiation pressure (SRP) along the trajectory. Instead, it is driven by a binary visibility signal, such as that provided by a Sun sensor, that indicates whether the Sun is in view or occluded. Consequently, the accuracy and reliability of the proposed method are unaffected by the inherently weak SRP signal, as the detection mechanism depends solely on discrete visibility states rather than on continuous dynamical forcing.

Then, the loss function is defined as the mean squared error (MSE) between the modeled states $\boldsymbol{x}_{\boldsymbol{\theta}}$ (computed integrating the dynamics with the neural event function) and the observed ones $\overline{\boldsymbol{x}}$:

$$\mathcal{L} = \sum_{j=0}^{T} \|\boldsymbol{x}_{j,\boldsymbol{\theta}} - \overline{\boldsymbol{x}}_j\|^2, \tag{4}$$

where $j$ indexes the time instances $t_j$ at which observations are available. The observed states may originate from actual trajectory measurements or high-fidelity simulations, such as those employing the Möller-Trumbore intersection algorithm.

The parameters of EclipseNET are updated by computing the gradient of the loss with respect to $\boldsymbol{\theta}$:

$$\nabla_{\boldsymbol{\theta}} \mathcal{L} = \sum_{i=1}^{n} \frac{\partial \mathcal{L}}{\partial x_i} \frac{\partial x_i}{\partial e_{\boldsymbol{\theta}}} \nabla_{\boldsymbol{\theta}} e_{\boldsymbol{\theta}}. \tag{5}$$

The first term follows directly from Eq. (4):

$$\frac{\partial \mathcal{L}}{\partial x_i} = 2 \sum_{j=1}^{T} (x_{ij,\boldsymbol{\theta}} - \overline{x}_{ij}). \tag{6}$$

The second term can be derived symbolically by first computing $\frac{\partial e_{\boldsymbol{\theta}}}{\partial x_i}$, while the third term is obtained by integrating Eq. (3) along with its

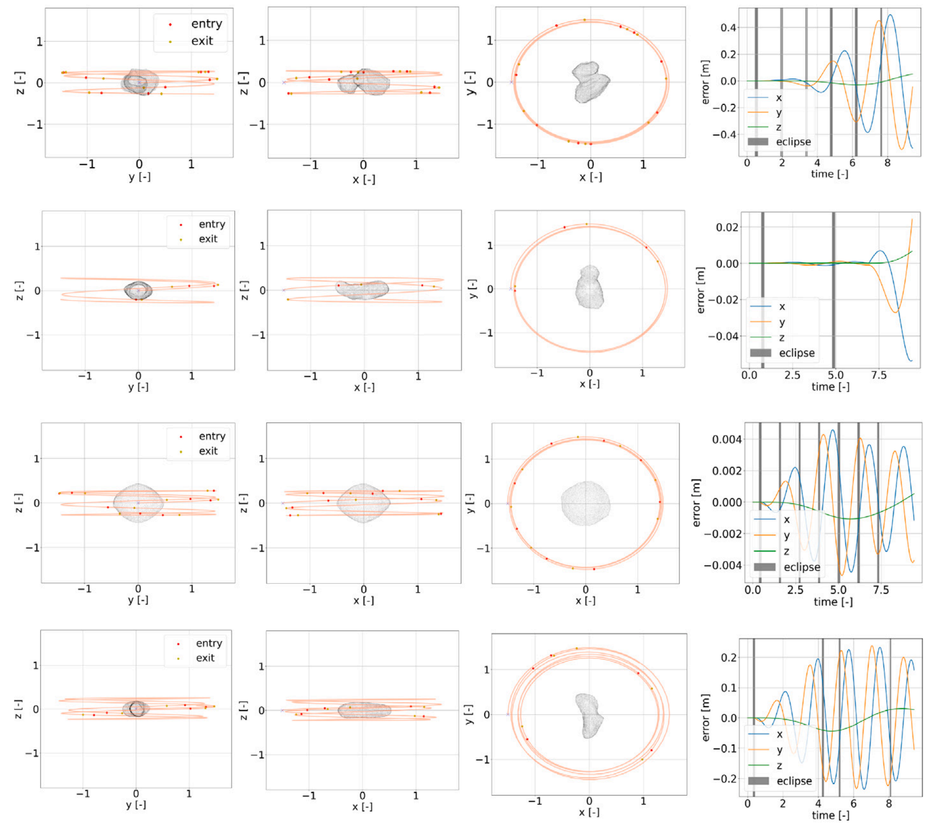

**Fig. 4.** *Left three columns*: three different projections of the three-dimensional orbits obtained using EclipseNET as an event; *right column*: positional coordinate errors between the trajectory computed with EclipseNET as an event and the one obtained using the Möller-Trumbore algorithm.

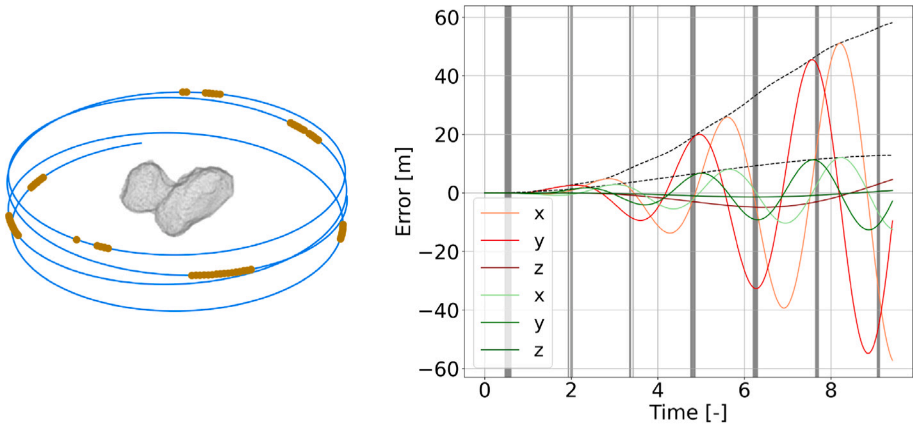

**Fig. 5.** *Left*: orbit around 67P/ Churyumov-Gerasimenko, with eclipse regions highlighted in dark yellow along the trajectory; *right*: error in the three positional components before (in red) and after (in green) the NeuralODE refinement. Eclipses are here displayed in gray. (For interpretation of the references to color in this figure legend, the reader is referred to the web version of this article.)

variational equations with respect to the parameters:

$$\begin{cases} \dot{\boldsymbol{x}} & = \boldsymbol{f}_{\boldsymbol{\theta}}(t, \boldsymbol{x}) \\ \dot{\epsilon}_{\boldsymbol{\theta}} & = g_{\boldsymbol{\theta}}(t, \boldsymbol{x}) \\ \dfrac{d}{dt}\left(\dfrac{\partial x_i}{\partial \theta_k}\right) & = \displaystyle\sum_{j=1}^{n} \dfrac{\partial f_{i,\boldsymbol{\theta}}}{\partial x_j}\dfrac{\partial x_j}{\partial \theta_k} + \dfrac{\partial f_{i,\boldsymbol{\theta}}}{\partial \theta_k} \\ \dfrac{d}{dt}\left(\dfrac{\partial e_{\boldsymbol{\theta}}}{\partial \theta_k}\right) & = \displaystyle\sum_{j=1}^{n} \dfrac{\partial g_{\boldsymbol{\theta}}}{\partial x_j}\dfrac{\partial x_j}{\partial \theta_k} + \dfrac{\partial g_{\boldsymbol{\theta}}}{\partial \theta_k}, \end{cases} \tag{7}$$

$\forall k = 1, \dots, m$. This results in a system of $(n+1)+(n+1)m$ equations to be integrated: we use the open-source *heyoka* software to both construct the variational equations and integrate them via Taylor method [32].

In the right panel of Fig. 5, we show the errors in the $x$, $y$, and $z$ positional components both before (in red) and after (in green) the NeuralODE refinement. The dashed black line in the same plot represents the norm of the error difference for both cases. The loss was computed using a single observation at the final time step of the simulation ($t_{obs} = 9.425$). The target state used for comparison was obtained using the Möller-Trumbore intersection algorithm: we depict the full orbit with the eclipses highlighted in dark yellow on the left side of Fig. 5. While it would in principle be feasible to learn the eclipse function from a large dataset of arbitrary eclipse detections using the NeuralODE framework, this is not the objective of the present study. Rather, we aim to demonstrate that the body silhouette as represented by an EclipseNET can be effectively improved by leveraging specific orbital regimes and trajectories, and hence using only limited, sparse data. This scenario is particularly relevant in operational contexts where the spacecraft is already in orbit around the asteroid, and eclipse events may be infrequent or irregular. Our results underscore EclipseNET's ability to adapt and generalize under data-scarce conditions, making it well-suited for in-situ refinement during mission operations.

The initial EclipseNET model was taken from the first epoch of the ReLU network discussed in Section 3 and shown in Fig. 3. Subsequently, the NeuralODE approach was used to minimize the error between the state predicted by the Möller-Trumbore algorithm and the state obtained using EclipseNET. This process resulted in a reduction of the error norm by nearly a factor of 7. As additional observations from diverse geometries are gathered, the representation of the small body's irregular silhouette progressively refines, enhancing the accuracy of trajectory predictions over time.

## 5. Conclusions

This work introduces a novel framework for modeling eclipse conditions around irregular small celestial bodies using neural implicit representations, with a focus on direct refinement from trajectory data using the recently popularized NeuralODEs framework. We first presented EclipseNET, a small neural network architecture designed to represent the complex and non-convex silhouettes of irregular bodies such as asteroids and comets. Extensive validation on four well-characterized targets (Bennu, Itokawa, 67P/Churyumov-Gerasimenko, and Eros) demonstrated that EclipseNET achieves higher accuracy and significantly greater computational efficiency than conventional ray-tracing techniques. Architecturally, SIREN-based models consistently outperformed ReLU-based networks, particularly in capturing the fine-grained features of eclipse boundaries. We then integrated EclipseNET within Taylor-based orbital propagators to enable precise and efficient eclipse event detection during trajectory simulation. Benchmarking against the Möller–Trumbore ray-tracing algorithm across multiple orbital scenarios showed that EclipseNET yields centimeter-level positional accuracy while achieving inference speeds exceeding traditional methods by over two orders of magnitude. To address the challenge of incomplete or uncertain shape models, we developed an online learning strategy based on NeuralODEs, which enables in-situ refinement of EclipseNET directly from trajectory data. This approach allows the eclipse model to improve incrementally as new observations are acquired, effectively compensating for deficiencies in a priori shape knowledge. Overall, our method provides a differentiable, data-efficient, and highly adaptive approach to eclipse prediction, supporting real-time, autonomous spacecraft operations in complex gravitational environments. Its compatibility with gradient-based optimization frameworks further facilitates integration into modern guidance, navigation, and control pipelines.

## CRediT authorship contribution statement

**Giacomo Acciarini:** Writing – review & editing, Writing – original draft, Visualization, Validation, Software, Methodology, Investigation, Formal analysis, Data curation, Conceptualization. **Dario Izzo:** Writing – review & editing, Software, Methodology, Conceptualization. **Francesco Biscani:** Software, Conceptualization.

## Declaration of competing interest

The authors declare that they have no known competing financial interests or personal relationships that could have appeared to influence the work reported in this paper.

## References

[1] C.M. Pieters, L.A. McFadden, Meteorite and asteroid reflectance spectroscopy: Clues to early solar system processes, Annu. Rev. Earth Planet. Sci. Vol. 22, Pp. 457- 497. 22 (1994) 457–497.

[2] J.-P. Sanchez, C. McInnes, Asteroid resource map for near-earth space, J. Spacecr. Rockets 48 (1) (2011) 153–165.

[3] A. Fujiwara, J. Kawaguchi, D. Yeomans, M. Abe, T. Mukai, T. Okada, J. Saito, H. Yano, M. Yoshikawa, D. Scheeres, et al., The rubble-pile asteroid itokawa as observed by hayabusa, Science 312 (5778) (2006) 1330–1334.

[4] S.-i. Watanabe, Y. Tsuda, M. Yoshikawa, S. Tanaka, T. Saiki, S. Nakazawa, Hayabusa2 mission overview, Space Sci. Rev. 208 (2017) 3–16.

[5] A.F. Cheng, A.S. Rivkin, P. Michel, J. Atchison, O. Barnouin, L. Benner, N.L. Chabot, C. Ernst, E.G. Fahnestock, M. Kueppers, et al., AIDA DART asteroid deflection test: Planetary defense and science objectives, Planet. Space Sci. 157 (2018) 104–115.

[6] P. Michel, M. Küppers, A.C. Bagatin, B. Carry, S. Charnoz, J. De Leon, A. Fitzsimmons, P. Gordo, S.F. Green, A. Hérique, et al., The ESA hera mission: detailed characterization of the DART impact outcome and of the binary asteroid (65803) didymos, Planet. Sci. J. 3 (7) (2022) 160.

[7] D. Scheeres, Orbital mechanics about small bodies, Acta Astronaut. 72 (2012) 1–14.

[8] S. Adhya, A. Sibthorpe, M. Ziebart, P. Cross, Oblate earth eclipse state algorithm for low-earth-orbiting satellites, J. Spacecr. Rockets 41 (1) (2004) 157–159.

[9] X. Jia, M. Xu, X. Pan, X. Mao, Eclipse prediction algorithms for low-earth-orbiting satellites, IEEE Trans. Aerosp. Electron. Syst. 53 (6) (2017) 2963–2975.

[10] V.K. Srivastava, J. Kumar, S. Kulshrestha, B.S. Kushvah, M. Bhaskar, S. Somesh, M. Roopa, B. Ramakrishna, Eclipse modeling for the mars orbiter mission, Adv. Space Res. 56 (4) (2015) 671–679.

[11] A. Lang, G. Chen, P. Guo, Heliotropic orbits at asteroid 99942 apophis: Considering solar radiation pressure and zonal gravity perturbations, Acta Astronaut. 198 (2022) 454–470.

[12] A. Lang, Spacecraft orbital stability zones around asteroid 99942 apophis, Acta Astronaut. 182 (2021) 251–263.

[13] J.W. McMahon, D.J. Scheeres, S.R. Chesley, A. French, D. Brack, D. Farnocchia, Y. Takahashi, B. Rozitis, P. Tricarico, E. Mazarico, et al., Dynamical evolution of simulated particles ejected from asteroid bennu, J. Geophys. Res.: Planets 125 (8) (2020) e2019JE006229.

[14] B. Neta, D. Vallado, On satellite umbra/penumbra entry and exit positions, J. Astronaut. Sci. 46 (1998) 91–103.

[15] D. Malyuta, Y. Yu, P. Elango, B. Açıkmeşe, Advances in trajectory optimization for space vehicle control, Annu. Rev. Control. 52 (2021) 282–315.

[16] C. Hergenrother, C. Maleszewski, M. Nolan, J.-Y. Li, C. Drouet d'Aubigny, F. Shelly, E. Howell, T. Kareta, M. Izawa, M. Barucci, et al., The operational environment and rotational acceleration of asteroid (101955) bennu from OSIRIS-REx observations, Nat. Commun. 10 (1) (2019) 1291.

[17] T. Möller, B. Trumbore, Fast, minimum storage ray/triangle intersection, in: ACM SIGGRAPH 2005 Courses, Association for Computing Machinery, 2005, pp. 7–es.

[18] F. Biscani, D. Izzo, Reliable event detection for taylor methods in astrodynamics, Mon. Not. R. Astron. Soc. 513 (4) (2022) 4833–4844.

[19] B. Mildenhall, P.P. Srinivasan, M. Tancik, J.T. Barron, R. Ramamoorthi, R. Ng, Nerf: Representing scenes as neural radiance fields for view synthesis, Commun. ACM 65 (1) (2021) 99–106.

[20] V. Sitzmann, J. Martel, A. Bergman, D. Lindell, G. Wetzstein, Implicit neural representations with periodic activation functions, Adv. Neural Inf. Process. Syst. 33 (2020) 7462–7473.

[21] G. Acciarini, F. Biscani, D. Izzo, Eclipsenets: a differentiable description of irregular eclipse conditions, in: Proceedings of SPAICE2024: The First Joint European Space Agency/IAA Conference on AI in and for Space, 2024, pp. 210–214.

[22] R.T.Q. Chen, Y. Rubanova, J. Bettencourt, D.K. Duvenaud, Neural ordinary differential equations, in: S. Bengio, H. Wallach, H. Larochelle, K. Grauman, N. Cesa-Bianchi, R. Garnett (Eds.), Advances in Neural Information Processing Systems, 31, Curran Associates, Inc., 2018, pp. 6572–6583, URL https://proceedings.neurips.cc/paper_files/paper/2018/file/69386f6bb1dfed68692a24c8686939b9-Paper.pdf.

[23] R.T.Q. Chen, B. Amos, M. Nickel, Learning neural event functions for ordinary differential equations, 2020, URL http://arxiv.org/abs/2011.03902.

[24] J.J. Park, P. Florence, J. Straub, R. Newcombe, S. Lovegrove, Deepsdf: Learning continuous signed distance functions for shape representation, in: Proceedings of the IEEE/CVF Conference on Computer Vision and Pattern Recognition, 2019, pp. 165–174.

[25] R. Gaskell, Eros polyhedral model, 2008, (available at https://sbn.psi.edu/pds/resource/erosshape.html).

[26] R. Gaskell, Itokawa polyhedral model, 2007, (available at https://darts.isas.jaxa.jp/planet/project/hayabusa/shape.pl).

[27] NASA/Goddard/University of Arizona, Bennu polyhedral model, 2020, (available at https://www.asteroidmission.org/updated-bennu-shape-model-3d-files).

[28] ESA/Rosetta/MPS, Churyumov-gerasimenko polyhedral model, 2014, (available at https://sci.esa.int/web/rosetta/-/54728-shape-model-of-comet-67p).

[29] D. Izzo, P. Gómez, Geodesy of irregular small bodies via neural density fields, Commun. Eng. 1 (1) (2022) 48.

[30] H. Si, TetGen, a delaunay-based quality tetrahedral mesh generator, ACM Trans. Math. Softw. ( TOMS) 41 (2) (2015) 1–36.

[31] R.T. Chen, D.K. Duvenaud, Neural networks with cheap differential operators, Adv. Neural Inf. Process. Syst. 32 (2019).

[32] F. Biscani, D. Izzo, Revisiting high-order taylor methods for astrodynamics and celestial mechanics, Mon. Not. R. Astron. Soc. 504 (2) (2021) 2614–2628, http://dx.doi.org/10.1093/mnras/stab1032.